ACS OMEGA

Article

Cite This: ACS Omega 2018, 3, 14526−14537

http://pubs.acs.org/journal/acsodf

Synthesis, Photophysics, and Switchable Luminescence Properties of a New Class of Ruthenium(II)−Terpyridine Complexes Containing Photoisomerizable Styrylbenzene Units

Poulami Pal,[†] Shruti Mukherjee,[†] Dinesh Maity,[†,‡] and Sujoy Baitalik*[,†]

[†]Department of Chemistry, Inorganic Chemistry Section, Jadavpur University, Kolkata 700032, India

[‡]Department of Chemistry, Katwa College, Purba Bardhaman, West Bengal 713130, India

Supporting Information

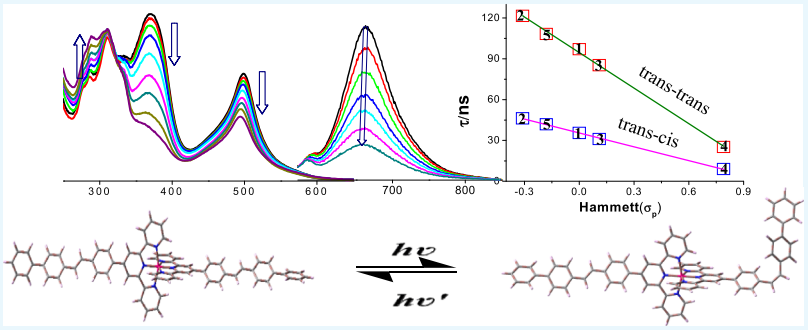

ABSTRACT: We report here the synthesis and structural characterization of a new class of homoleptic terpyridine complexes of Ru(II) containing styrylbenzene moieties to improve room-temperature luminescence properties. Solid-state structure determination of **2** was done through single-crystal X-ray diffraction. Tuning of photophysical properties was done by incorporating both electron-donating and electron-withdrawing substituents in the ligand. The complexes exhibit strong emission having lifetimes in the range of 10.0−158.5 ns, dependent on the substituent and the solvent. Good correlations were also observed between Hammett σ_p parameters with the lifetimes of the complexes. Styrylbenzene moieties in the complexes induce trans−trans to trans−cis isomerization accompanied by huge alteration of their spectral profiles upon treating with UV light. Reversal of trans−cis to trans−trans forms was also achieved on interacting with visible light. Change from trans−trans to the corresponding trans−cis form leads to emission quenching, whereas trans−cis to the corresponding trans−trans form leads to restoration of emission. In essence, "on−off" and "off−on" photoswitching of luminescence was observed. Calculations involving density functional theory (DFT) and time-dependent-DFT methods were performed to understand the electronic structures as well as for appropriate assignment of the absorption and emission bands.

INTRODUCTION

Compounds with photoswitchable optical and luminescence properties are very promising with regard to their important roles in various applications such as optical materials, photoswitches, and memory devices.[1−7] Significant efforts have been made to strengthen this area, and as an outcome, a sizable number of photochromic systems based on azobenzenes, stilbenes, diarylethenes, spiropyrans, and spirooxazines have been developed.[8−13] Despite numerous reports on photoisomerizable organic compounds where the photochromic activity originated from their singlet excited state, only a limited number of studies have been performed on their inorganic counterparts (coordination complexes).[14−24] Transition-metal based materials are especially attractive in that they have additional advantage over their organic counterparts in offering tunability in the electronic nature of both inorganic and organic components.[25−29] In addition, incorporation of photoisomerizable ligands (such as stilbene and azobenzene) onto the complex systems with various transition metals induces the access of the ligand-centered triplet state leading to the generation of long-lived excited states. Moreover, the excitation and emission wavelengths could be extended to a long wavelength region.[2,14,30−37]

Among numerous transition metals, Ru(II)−polypyridine complexes are regarded as potential building blocks for photomolecular devices because of their remarkable photoredox behaviors and long-lived metal-to-ligand charge-transfer (MLCT) excited states.[38−41] Polypyridine ligands based on bipyridine units (such as $[Ru(bpy)_3]^{2+}$) are better over terpyridine (such as $[Ru(tpy)_2]^{2+}$) with regard to their emission behaviors, while terpyridine units are better in terms of construction of linear and achiral octahedral architectures.[42−47] $[Ru(bpy)_3]^{2+}$ exhibits intense and long-lived ($\tau \approx 1\ \mu s$) luminescence,[38] whereas $[Ru(tpy)_2]^{2+}$ is

Received: August 7, 2018
Accepted: October 19, 2018
Published: October 31, 2018

DOI: 10.1021/acsomega.8b01927
ACS Omega 2018, 3, 14526−14537

almost nonemissive with excited-state lifetime ($\tau \approx 0.25$ ns) at room temperature (RT).[48] The lack of emission is due to the close proximity of ^{3}MLCT and ^{3}MC state induced by their distorted octahedral geometries.[42−47] For proper utilization of the structurally appealing terpyridine complexes of Ru(II) as effective visible light photosensitizers, their luminescence behaviors have to be optimized. Improvement of emission characteristics can usually be achieved by synthetic strategies, viz. upon incorporation of electron-donating or electron-accepting substituents[48−51] and polyaromatic chromophores[52−54] to adjust the relative position of ^{3}MLCT and ^{3}MC states. Cyclometalated ligands can often destabilize the ^{3}MC state.[55−58] Replacement of pyridine ring by different heterocyclic moieties may sometime give rise to less distorted octahedral configuration.[59−63] The important point for improving their emission behaviors is to extend the electron delocalization for minimizing nonradiative deactivation channels.[64−71]

As a part of continuous efforts for the design and improving the luminescence properties of Ru(II)−terpyridine complexes,[72−81] we report in this work synthesis, characterization, photophysics, redox behaviors, and trans−cis photoisomerization process of a new class of homoleptic complexes of the type $[Ru(tpy\text{-}pvp\text{-}X)_2](ClO_4)_2$ by introducing styrylbenzene units onto the terpyridine moiety (Chart 1). The electronic nature

Chart 1. Molecular Structures of Heteroleptic Ru(II)−Terpyridine Complexes

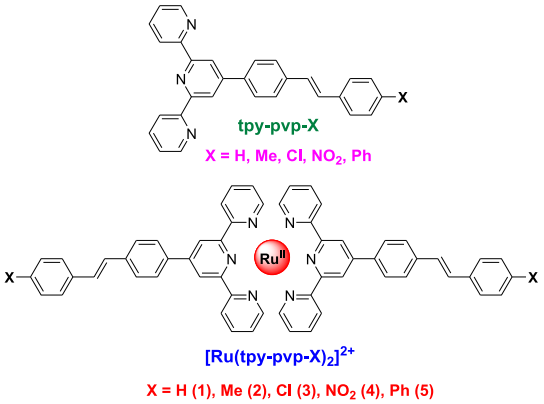

of X in tpy-pvp-X was varied to tune the properties as well as the kinetics of the isomerization process. Photoisomerization studies of some Ru(II) complexes incorporating azo functionality onto the terpyridine moiety are reported.[14,15,82−88] However, to our notice, no such studies were carried out by incorporating styrylbenzene unit into the terpyridine motif. Prior to this work, we recently reported a heteroleptic series of the type $[(tpy\text{-}PhCH_3)Ru(tpy\text{-}pvp\text{-}X)](BF_4)_2$ with the same styrylbenzene−terpyridine ligands.[89] Incorporation of two styrylbenzene units around the central Ru(II) center could extend the path of electron delocalization substantially. It is expected that lengthening of conjugation will enhance the lifetime of the present series with respect to the previous one. In addition, presence of two photoisomerizable styrylbenzene units in the present series of complexes could also facilitate the occurrence of photoinduced trans−trans to trans−cis isomerization processes. In practice, the lifetime of the complexes in this study enhanced substantially with respect to the previous one. Finally, insights into the electronic structures of the trans−trans, trans−cis, and cis−cis forms of complexes and appropriate assignment of their optical spectral bands were obtained by density functional theory (DFT) and time-dependent TD-DFT calculations.

RESULTS AND DISCUSSION

Synthesis and Characterization. Homoleptic bis-terpyridine Ru(II) complexes were synthesized in a straightforward manner by the reaction between $RuCl_3{\cdot}3H_2O$ and the respective terpyridine ligand (tpy-pvp-X) in 1:2 proportion in refluxing $(CH_2OH)_2$ under argon protection. Column chromatography and recrystallization techniques were employed to purify the complexes. Characterization of the complexes was conducted using standard analytical and spectroscopic tools, and the data are given in the Experimental Section. Single-crystal X-ray structure of **2** was also determined.

Nuclear Magnetic Resonance Spectra. Figure 1 displays the ^{1}H NMR spectra of **1**−**5**. Tentative assignment of proton

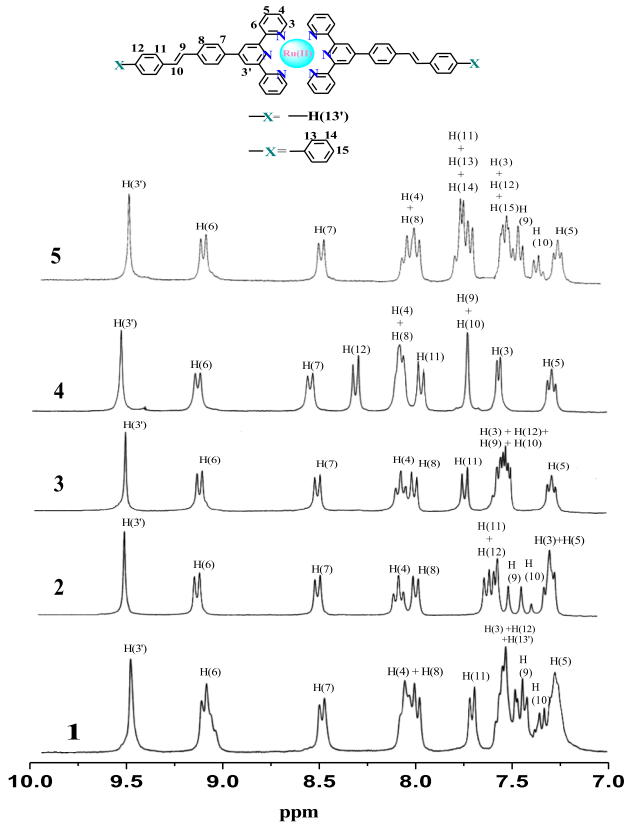

Figure 1. ^{1}H NMR spectra along with the assignment of peaks of **1**−**5** in DMSO-d_6.

resonances is also given in Figure 1. The $\{^1H-^1H\}$ COSY nuclear magnetic resonance (NMR) spectra (Figures S1−S5, Supporting Information) along with the spectral data of structurally related complexes guide us for the assignment of proton resonances in the complexes.[75−80] The relatively simple ^{1}H NMR spectra reflect a symmetrical environment around the Ru(II) center of the complexes. The singlet that appears at the most downfield region (~9.5 ppm) is assigned as H3′. A pair of doublet within 7.32−7.72 ppm is assignable to the protons of ethylenic double bond (H9 and H10) and corresponds to the trans−trans conformation. In some cases, they appeared

DOI: 10.1021/acsomega.8b01927
ACS Omega 2018, 3, 14526−14537

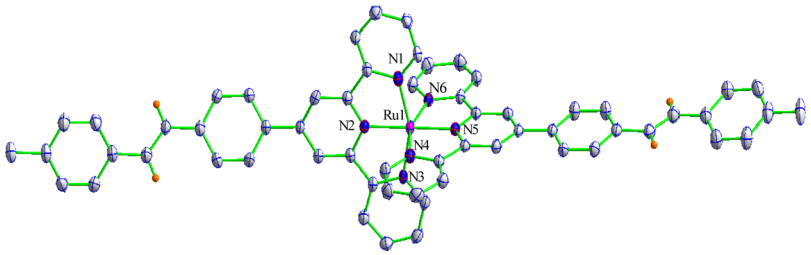

Figure 2. Perspective view for 2^{2+} showing 50% probability of thermal ellipsoids.

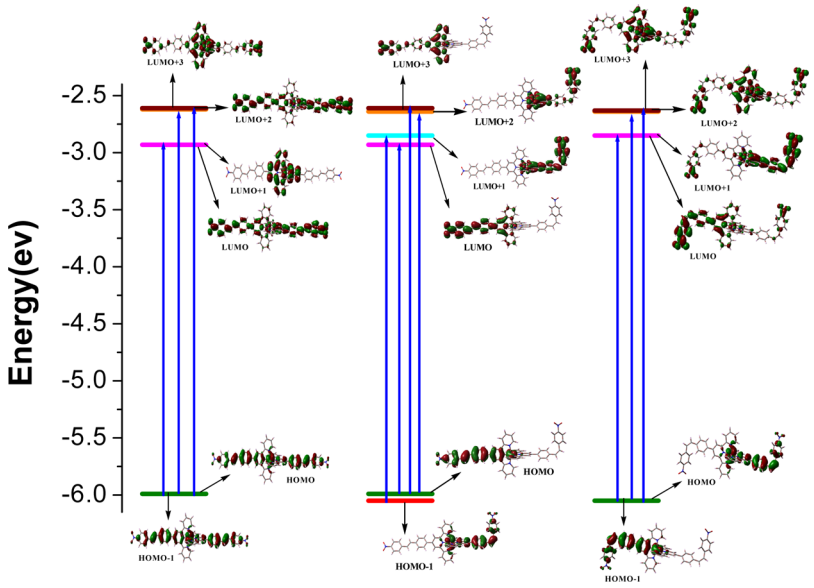

Figure 3. Energy-level diagram showing dominant transitions involved in the lowest-energy absorption band in trans−trans (left panel), trans−cis (middle panel), and cis−cis (right panel) forms of $[Ru(tpy\text{-}pvp\text{-}NO_2)_2]^{2+}$ (**4**) in MeCN.

within the multiplet because of the coincidence of other protons. The singlet at 2.5 ppm for **2**, which is not shown in Figure 1, corresponds to the $-CH_3$ groups.

Mass Spectra. Electrospray mass spectra along with the isotopic distributions for **1**−**5** are presented (Figures S6−S10, Supporting Information). In all cases, an abundant peak is observed between m/z = 462.03 for **1** and 538.29 for **5** with a good correlation between experimental and simulated patterns. The successive isotopic lines in the mass spectra are separated by 0.5 Da, which clearly show the existence of $[Ru(tpy\text{-}pvp\text{-}X)_2]^{2+}$ type of species in all cases. The complexes also exhibit a monopositive ion, $[Ru(tpy\text{-}pvp\text{-}X)_2(ClO_4)]^{+}$, in some cases, but the abundance of these species is extremely small compared with +2 charged species (Figures S11−S13, Supporting Information).

Crystal Structure of 2. Single crystals were acquired by layering toluene to the MeCN−dichloromethane (DCM) (1:1 v/v) solution of **2**. Relevant data related to crystal structure determination are tabulated in Table S1 (Supporting Information). Selected bond distances and angles are summarized in Table S2 (Supporting Information). A perspective view of **2** is presented in Figure 2. The geometry of **2** around the metal center is distorted octahedrally. Trans−trans orientation of two aryl units across the double bond at both sides of the Ru(II) center is also evident from the structure. The Ru−N bond lengths varying between 1.971(2) and 2.080(2) Å are comparable to those of the reported structurally related compounds.[79−81]

Computational Studies. Geometries of trans−trans, trans−cis, and cis−cis forms were optimized with the DFT method using Gaussian 09 software in acetonitrile. Optimized structural details are presented in the Supporting Information (Figure S14 and Tables S2−S6). Distorted octahedral geometry of the complexes with two tpy units oriented meridionally around the metal center is evident from the structural parameters. In the case of **2**, experimental structural parameters agree with the calculated values.

The molecular orbitals (MOs) and their energies are given in the Supporting Information (Figures S15−S19 and Tables S7−S11). With few exceptions, highest occupied molecular orbitals (HOMOs) in all the three forms are mainly localized on the Ru(II) center and styrylbenzene group, whereas the lowest unoccupied molecular orbitals (LUMOs) are localized on the terpyridine units. By contrast, lowest-energy LUMO in **4** is located on the nitrobenzene part because of its electron-withdrawing nature, whereas higher-energy LUMOs are localized as usual on both terpyridine and nitrobenzene moieties of the ligand. In general, the compositions of HOMOs and LUMOs in three geometrical forms of the complexes are similar, and only a small variation is observed in some cases. The electrostatic potential energy plots of **1**−**5** showing spreading of electron density are presented in Figure S20 (Supporting Information). Green color stands for the electron-rich portion, whereas blue color stands for the electron-deficient portion. Distribution of electronic charge

DOI: 10.1021/acsomega.8b01927
ACS Omega 2018, 3, 14526−14537

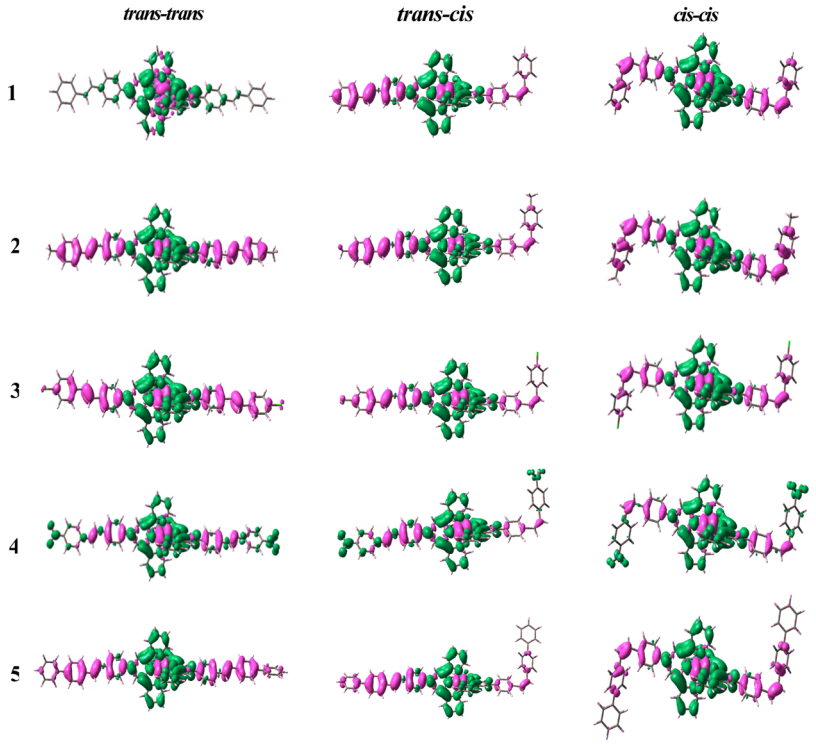

Figure 4. Difference in electron density upon excitation from the ground S_0 state to the lowest-energy singlet excited state in both trans−trans, trans−cis, and cis−cis forms of **1**−**5**. Green and magenta color shows the regions of increasing and decreasing and increasing electron density, respectively.

Table 1. Emission Maxima of 1−5 in MeCN According to UKS Calculations and Associated Experimental Values

	before photolysis		after photolysis		
	λ_{expt}/nm	λ_{cal} (trans−trans)/nm	λ_{expt}/nm	λ_{cal} (trans−cis)/nm	λ_{cal} (cis−cis)/nm
1	661	635	652	632	628
2	666	644	659	639	629
3	664	634	657	631	627
4	670	639	661	634	629
5	667	638	660	633	630

density does not differ significantly among the three forms as expected.

Calculated UV−vis spectra of trans−trans, trans−cis, and cis−cis forms of complexes were obtained by carrying out the TD-DFT calculation in an acetonitrile medium utilizing the conductor-like polarizable continuum model. The spectral data of singlet−singlet transitions in the three forms of **1**−**5** and their band assignment were given in the Supporting Information (Tables S12−S16). The set of MOs participated in the longest-wavelength band are displayed in Figures 3 and S21−S24 (Supporting Information). Lowest-energy band located between 487 nm (**3** and **4**) and 501 nm (**5**) in their trans−trans forms, between 482 nm (**3** & **4**) and 496 nm (**5**) in their trans−cis forms, and between 474 nm (**3**) and 482 nm (**5**) in their cis−cis forms arises because of combined Ru(II)-to-terpyridine MLCT and styrylbenzene-to-terpyridine intraligand charge-transfer (ILCT) (Figures S21−S24, Supporting Information). In the case of **4**, the band at 487 nm is due to combined charge transfer from ruthenium(II) and styrylbenzene unit to nitrobenzene moiety (Figure 3). Thus, the lowest-energy band has both MLCT and ILCT characters. The band that is located between 303 and 373 nm considering all the three forms is mainly because of the charge transfer from styrylbenzene to terpyridine moiety. The high-intensity UV bands mainly comprise $\pi-\pi^*$ transitions between the aromatic and terpyridine units of tpy-pvp-X. Small blue shift of MLCT and ILCT bands is observed on passing from trans−trans to trans−cis and finally to cis−cis forms. Further insight for the assignment of bands are obtained from natural transition orbital (NTO) analysis (Figures S25−S27, Supporting Information) and electron density difference map (EDDM) (Figure 4). Both NTO and EDDM plots again confirm that the band at lowest energy is an admixture of MLCT as well as ILCT characters.

UKS calculations helped to get some insight about their emission spectral properties. Optimized geometries and metrical parameters are given in Figure S28 and Tables S2−S6 (Supporting Information). Theoretical emission band varies between 634 (**3**) and 644 nm (**2**) for trans−trans, between 631 (**3**) and 639 nm (**2**) for trans−cis, and between 627 (**3**) and 630 nm (**5**) for cis−cis forms, depending the electronic nature of X in the complexes (Table 1).

Electrochemical Behaviors. The electrochemical data of **1**−**5** in acetonitrile are given in the Supporting Information (Table S17). The representative cyclic voltammogram of **1** is displayed in the Supporting Information (Figure S29). The

DOI: 10.1021/acsomega.8b01927
ACS Omega 2018, 3, 14526−14537

Table 2. Photophysical Parameters of 1−5

			luminescence				
compds		absorption λ_{max}/nm (ε, M^{-1} cm^{-1})	λ_{max}/nm	τ	Φ	k_r/s^{-1}	k_{nr}/s^{-1}
1	MeCN (298 K)	495(32 350), 355(sh)(39 510), 331(sh)(52 540), 311(62 720)	658	τ_1 = 4.0 ns, τ_2 = 54.5 ns	0.86×10^{-3}	2.1×10^5, 1.6×10^4	2.5×10^8, 1.8×10^7
2		497(27 050), 357(40 450), 333(sh)(41 400), 311(45 170)	659	τ_1 = 6.0 ns, τ_2 = 67.7 ns	1.05×10^{-3}	1.7×10^5, 1.5×10^4	1.7×10^8, 1.5×10^7
3		496(30 640), 356(47 950), 333(sh)(51 450), 311(40 270)	660	τ_1 = 3.8 ns, τ_2 = 52.1 ns	0.82×10^{-3}	2.2×10^5, 1.6×10^4	2.6×10^8, 1.9×10^7
4		498(37 070), 368(57 060), 335(sh)(44 420), 309(47 060)	669	τ_1 = 1.4 ns, τ_2 = 10.0 ns	0.68×10^{-3}	4.9×10^5, 6.8×10^4	7.1×10^8, 9.9×10^7
5		497(33 150), 360(52 720), 332(sh)(49 790), 311(54 650)	664	τ_1 = 5.8 ns, τ_2 = 64.3 ns	0.95×10^{-3}	1.6×10^5, 1.5×10^4	1.7×10^8, 1.6×10^7
1	DMSO (298 K)	502(42 570), 363(sh)(49 560), 337(sh)(66 130), 316(74 630)	669	τ_1 = 19.0 ns, τ_2 = 135.6 ns	0.93×10^{-3}	4.9×10^4, 6.9×10^3	5.3×10^7, 7.4×10^6
2		506(34 950), 364(47 650), 338(sh)(50 350), 318(53 520)	672	τ_1 = 24.0 ns, τ_2 = 158.5 ns	1.03×10^{-3}	4.3×10^4, 6.5×10^3	4.2×10^7, 6.3×10^6
3		505(35 010), 363(61 820), 339(sh)(60 980), 318(59 560)	672	τ_1 = 18.1 ns, τ_2 = 130.0 ns	0.83×10^{-3}	4.6×10^4, 6.4×10^3	5.5×10^7, 7.7×10^6
4		507(53 550), 379(64 280), 339(sh)(58 220), 314(67 260)	679	τ_1 = 3.0 ns, τ_2 = 43.0 ns	0.70×10^{-3}	2.3×10^5, 1.6×10^4	3.3×10^8, 2.3×10^7
5		506(45 470), 370(64 940), 336(sh)(62 670), 315(67 750)	673	τ_1 = 23.0 ns, τ_2 = 145.8 ns	0.95×10^{-3}	4.1×10^4, 6.5×10^3	4.3×10^7, 6.9×10^6
1	MeOH/EtOH (1/4) (77 K)		647	42.5 μs	0.42	9.8×10^3	1.4×10^4
2			653	47.3 μs	0.51	1.1×10^4	1.0×10^4
3			651	42.1 μs	0.39	9.3×10^3	1.5×10^4
4			660	35.2 μs	0.32	9.1×10^3	1.9×10^4
5			657	45.5 μs	0.47	1.0×10^4	1.2×10^4

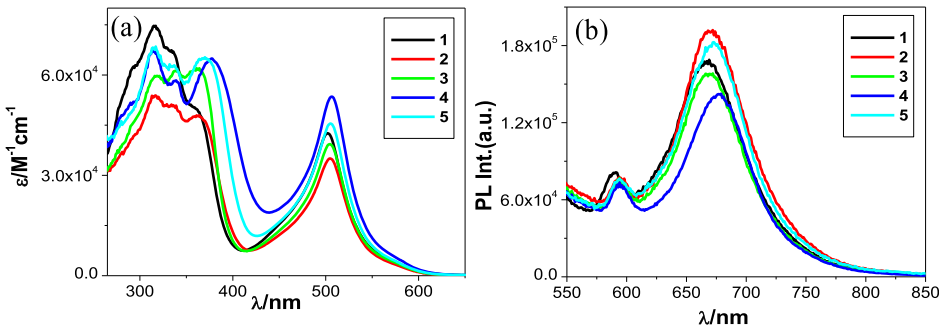

Figure 5. UV−vis absorption (a) and emission (b) spectra of complexes (**1**−**5**) in DMSO.

reversible wave at around 1.28 V is due to oxidation of Ru^{II} to Ru^{III} in the complexes. On the other hand, the waves observed in the range of −0.91 to −1.47 V are due to the reductions of terpyridine units as well as for NO_2 group (for **4**). Cyclic voltammogram for the reduction side of the nitro compound (**4**) is interesting and quite different from the rest of the series (Figure S30, Supporting Information), and complex **4** exhibits three successive reduction waves between −0.91 and −1.47 V, whereas the remaining complexes show two reduction waves between −1.03 and −1.40 V. Thus, first reduction for **4** corresponds to the reduction of the nitro groups within the complex. Electrochemical behaviors were also supported by DFT-calculated results. Spin density calculations have also been done and relevant plots are presented in Figure S31 (Supporting Information). Spin density was predominantly localized on Ru in the one-electron oxidized form, while on terpyridine moiety upon reduction with the exception of **4**, for which the density is mostly localized on nitrobenzene unit in the reduction process.

Absorption Spectra. Absorption spectral characteristics of the compounds were studied in both acetonitrile and dimethyl sulfoxide (DMSO) and relevant spectral data are collected in Table 2, whereas corresponding profiles are displayed in Figures 5a and S32a (Supporting Information). The spectral pattern is very similar, and each of them shows a number of intense bands in both UV and visible domain. Experimental data of structurally related complexes and results of TD-DFT computation indicate that the band within 495 and 507 nm is a combination of $^1[Ru^{II}(d)^6] \rightarrow {}^1[Ru^{II}(d)^5$tpy-pvp-X($\pi^*$)$^1]$ MLCT and ILCT transitions. The band within 355 and 379 nm mainly comprises ILCT transitions, whereas very intense UV bands arise from $\pi-\pi^*$ transitions in aromatic and heteroaromatic moieties of tpy-pvp-X ligands. The correlation among the calculated and experimental data is usually good. MLCT band is shifted to a longer wavelength with respect to $[Ru(tpy)_2]^{2+}$ (474 nm)[38] as styrylbenzene units induce extensive electronic delocalization toward the terpyridine unit. In addition, the peak position of both MLCT and ILCT band varies with the nature of X.

Emission Properties. At RT, both emission spectra and luminescence lifetimes were recorded in acetonitrile and DMSO, while at 77 K, the same measurements were

DOI: 10.1021/acsomega.8b01927
ACS Omega 2018, 3, 14526−14537

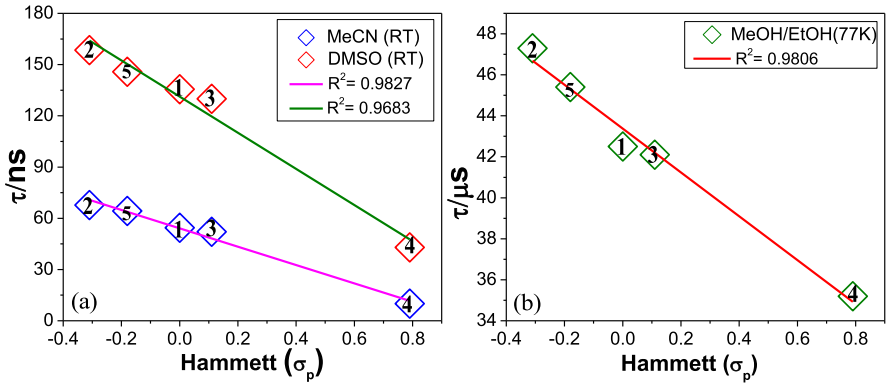

Figure 6. Plot of lifetime of **1**−**5** vs Hammett σ_p parameters at RT (a) and at 77 K (b).

performed in EtOH−MeOH glass (4:1, v/v). Relevant photophysical parameters are mentioned in Table 2, and corresponding emission spectra are displayed in Figures 5b and S32b (Supporting Information). Irradiation at MLCT results a moderately strong luminescence band with their peak maximum varying between 658 (**1**) and 669 nm (**4**) in acetonitrile and between 669 (**1**) and 679 nm (**4**) in DMSO at RT. It is to be noted that a small overlapping band at ∼590 nm is visible in all cases, which is probably due to the phosphorescence from the $^3\pi,\pi^*$ state of styrylbenzene moiety. The possibility of ligand impurity is completely ruled out as free tpy-vpv-X ligands exhibit fluorescence from the $^1\pi,\pi^*$ state within the range of 400−420 nm. We have deconvoluted the emission spectra of the complexes to obtain an individual spectrum (Figures S33−S34, Supporting Information), and radiative and nonradiative rate constant values that are provided in Table 2 are based on deconvoluted spectra. At 77 K, the emission maximum within 647 (**1**) and 660 nm (**4**) is blue-shifted along with the significant enhancement of both emission intensity and quantum yields (Figure S35, Supporting Information).

The lifetime of complexes varied between 10.0 (**4**) and 67.7 ns (**2**) in acetonitrile (Figure S36, Supporting Information), whereas in DMSO, the lifetimes increased substantially with their values lying between 43.0 (**4**) and 158.5 ns (**2**) (Figure S37, Supporting Information). Like MLCT absorption maximum, emission peak also varies with the electronic nature of X, but no linear correlation is obtained between the emission energy and the Hammett σ_p parameters. By contrast, the lifetime of the complexes increases systematically upon increasing the electron-donating nature of X yielding a linear plot between the lifetime and Hammett σ_p parameters in both acetonitrile and DMSO at RT (Figure 6a). In a frozen matrix, enhancement of lifetime is enormous compared to the fluid solution for all the complexes as expected, and the observed lifetime was found to lie between 35.2 (**4**) and 47.3 μs (**2**) at 77 K (Figure S38, Supporting Information). Interestingly, 77 K emission lifetime of the complexes also vary systematically with the electronic nature of X, and a reasonably good linear correlation was found between the lifetime and Hammett σ_p parameters (Figure 6b).[80,90]

The complexes exhibit biexponential decay in both acetonitrile and DMSO at RT. It is probable that the initial short component accounts for deactivation of the ^{3}MLCT state, whereas the long-lived species arises from the equilibrated triplet state of ^{3}MLCT and styrylbenzene units. The emission profiles of complexes at 77 K exhibit clean vibrational progression with their spacing in the range of 1224−1372 cm^{-1}, indicating substantial participation of the triplet ligand-centered emission (Figure S35, Supporting Information). The emission maxima at 77 K also give rise to the estimate of their zero−zero spectroscopic energy (E_{00}) and estimated values were found to vary between 1.88 and 1.92 eV, depending on the nature of X in the complexes. Thus, an interesting and significant aspect is the design of new Ru(II)−terpyridine complexes that exhibit moderately strong emission at RT with their lifetimes varying between 10.0 and 158.5 ns. In our previous report, we showed that incorporation of one styrylbenzene−terpyridine conjugate leads to the enhancement of lifetime up to 22.82 ns in a related heteroleptic series where the extent of enhancement was 2 orders of magnitude higher than the $[Ru(tpy)_2]^{2+}$ complex (τ = 0.25 ns).[48] In the present series of homoleptic complexes, incorporation of two styrylbenzene−terpyridine ligands around the Ru(II) center provides greater electron delocalization in the excited state, resulting in a substantial increase of the lifetime at RT and the extent of enhancement is about 3 orders of magnitude higher compared with the parent $[Ru(tpy)_2]^{2+}$ (τ = 0.25 ns). Moreover, their lifetimes also systematically varied with the electronic nature of X, yielding a good correlation with Hammett σ_p parameters.

Photoisomerization Studies. Because of the presence of two photoisomerizable C═C units, each complex undergoes trans−cis isomerization induced by light. Photoisomerization was initially performed in both acetonitrile and DMSO as most of the photophysical and electrochemical studies were carried out in these solvents. As the isomerization process is very slow in these solvents, we use 1:50 (v/v) acetonitrile−DCM mixture for the purpose of photoisomerization studies. Irradiation of the solution of complexes with UV light induces a systematic and substantial UV−vis absorption spectral change in all cases with clean and well-defined isosbestic point in each case as displayed in Figures 7a,c,e and S39 (Supporting Information). During photolysis, both MLCT and ILCT bands gradually lose their intensities, although the extent of decrease of the ILCT band is more pronounced than the MLCT band in all cases. The decrease of MLCT and ILCT band intensities is accompanied by the increase of intensity of $\pi-\pi^*$ bands. The extent of decrease varies between 30 and 45% for the MLCT band and between 70−88% for the ILCT band (in the range of 360−380 nm), while the extent of increase of $\pi-\pi^*$ band at ∼290 nm varies between 30 and 75% in the complexes. The time required to reach the saturation point vary between 170 m (**1**) and 300 m (**4**), depending on

DOI: 10.1021/acsomega.8b01927
ACS Omega 2018, 3, 14526−14537

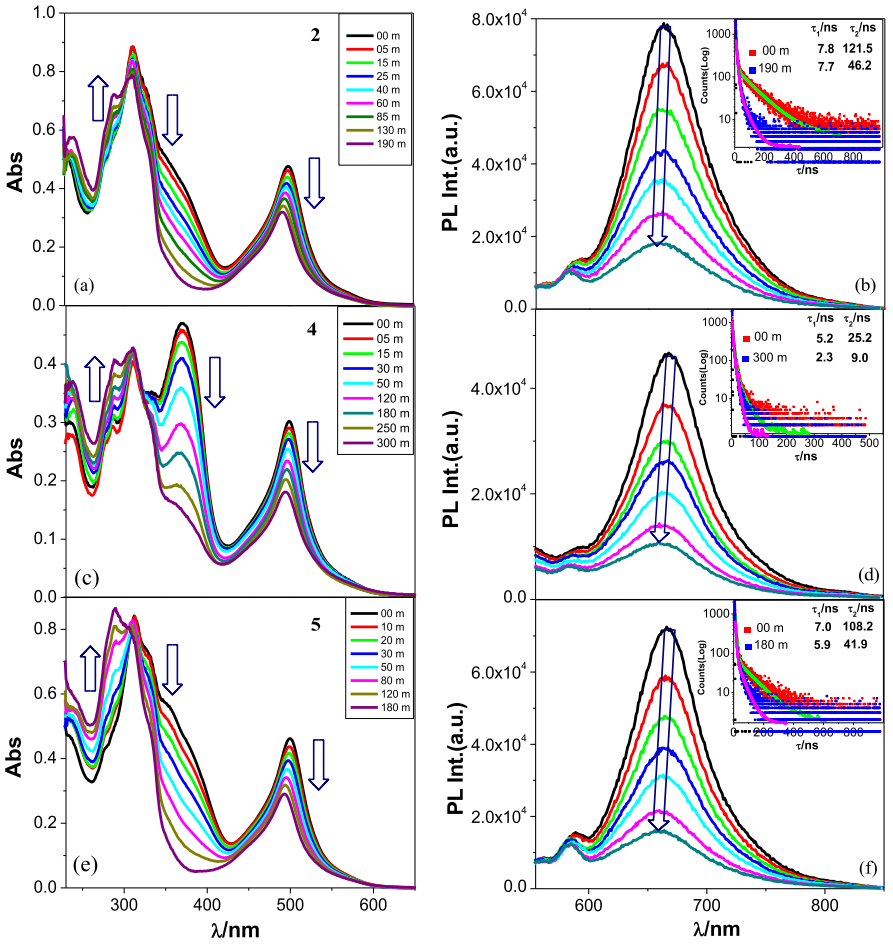

Figure 7. Changes in absorption and luminescence (λ_{ex} = 500 nm) spectra of **2** (a,b, respectively), **4** (c,d, respectively), and **5** (e,f, respectively) in MeCN−DCM (1:50 v/v) upon excitation with UV light. Changes in lifetime upon photolysis are shown in the insets.

the electronic property of X. Small but finite blue shift of the MLCT band was noticed for all complexes upon photolysis. The reverse process also occurs on irradiation with visible light, but the rate is extremely slow compared with the forward process. Upon irradiation with UV light, almost complete quenching (∼80%) accompanied with small blue shift of emission band was noticed in all complexes (Figures 7b,d,f and S39, Supporting Information). Reverse process upon interaction with visible light again restores the original emission. Interestingly, "on−off" and "off−on" switching of emission is feasible on treating with UV and visible light successively.

The observed spectral change is associated with the conversion of either one or both styrylbenzene units from the trans- to the cis-form that is either from initial trans−trans to trans−cis or to the cis−cis form in the complexes. In order to understand the mode of isomerization process, we also acquired the ^{1}H NMR spectrum of **2** in DMSO-d_6−$CDCl_3$ (1:4, v/v) after photolysis of ∼10 h (Figure 8). It is observed that H9 and H10 protons associated with ethylenic double bond as well as H7, H8 H11, and H12 protons adjacent to the double bond are shifted toward the upfield region, albeit in small extent. In the initial trans−trans orientation, H9 and H10 protons associated with ethylenic double bond appeared in the range of 7.07−6.96 ppm with the value of coupling constant J ≈ 16 ppm. The spectrum obtained after photolysis shows two doublet signals within the range of 6.72−6.64 ppm with J ≈ 12 ppm, indicating the signature of *cis*-olefinic hydrogens. In

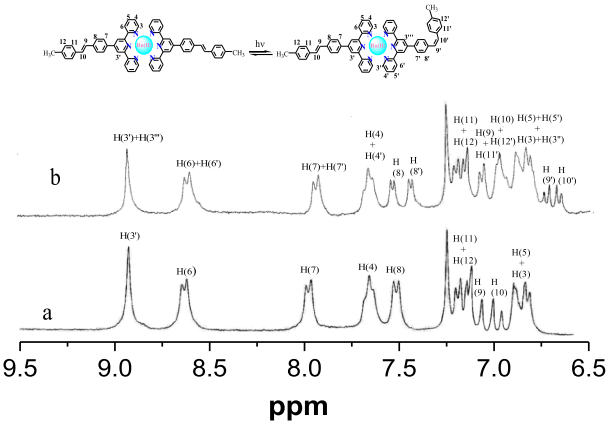

Figure 8. ^{1}H NMR spectra of $[Ru(tpy\text{-}pvp\text{-}Me)_2]^{2+}$ (**2**) in DMSO-d_6−$CDCl_3$ (1:4, v/v) before (a) and after photolysis with UV light (b).

addition, unresolved overlapping features are also observed in the range of 7.08−6.93 ppm because of the coexistence of H9, H10, H11′, and H12′ protons. Thus, ^{1}H NMR spectral studies suggest that photoisomerization involves the conversion from trans−trans to trans−cis form.

In previous section, we have performed TD-DFT as well as UKS calculations in three forms of the complexes. The experimentally observed position of MLCT absorption and

DOI: 10.1021/acsomega.8b01927
ACS Omega 2018, 3, 14526−14537

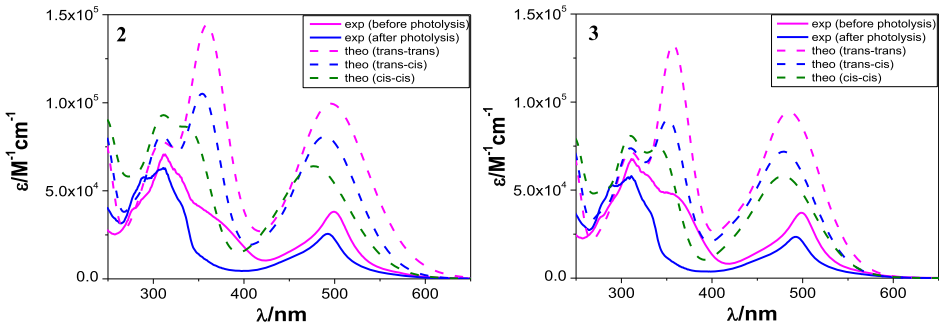

Figure 9. Calculated {dashed lines: trans−trans (pink), trans−cis (blue), and cis−cis (green)} and observed (solid lines) absorption spectra of **2** and **3** in MeCN.

luminescence band after photolysis correlates better with trans−cis forms compared with their cis−cis orientation (Tables 1, S12−S16, Figures 9, and S40−S42 Supporting Information). Thus, both experimental observation and theoretical calculations suggest conversion from trans−trans to the corresponding trans−cis forms upon irradiation with UV light for all complexes.

In line with steady-state spectra, decrease in lifetime (∼65%) was also observed for all these compounds upon photolysis. It should be mentioned that the lifetime of complexes in acetonitrile−DCM (1:50, v/v) is much higher (varying between 25.2 ns (**4**) and 121.5 ns (**2**)) compared with neat MeCN, while little less compared with DMSO. Moreover, linear correlation is observed upon plotting lifetimes of both trans−trans and trans−cis forms and Hammett σ_p parameters (Figure 10). It is to be noted that the lifetime of the complexes

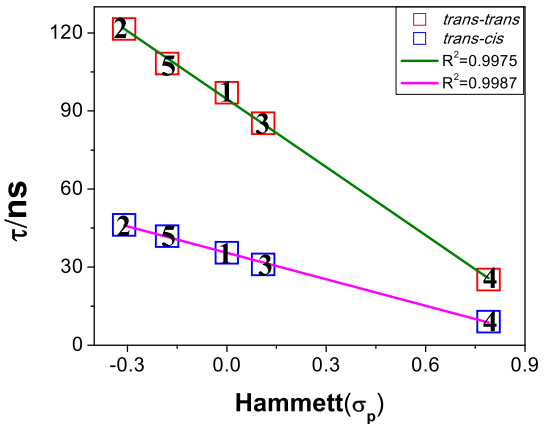

Figure 10. Plot of lifetime of the complexes (both trans−trans and trans−cis forms) in MeCN−DCM (1:50, v/v) vs Hammett σ_p parameters with linear least square fits to the data.

increases systematically upon increasing the electron donating capability of X (Figures 6 and 10). Although the actual cause of this trend cannot be explained with a clear view, the substituent X probably affects $^3\pi,\pi^*$ or ^{3}ILCT state to a greater extent compared with the ^{3}MLCT state in the complexes. We suggested that the biexponential decay profiles indicated the coexistence of ^{3}MLCT and ^{3}ILCT or $^3\pi,\pi^*$ excited states under equilibrium at RT. It is expected that with an electron donating substituent, the energy difference between ^{3}MLCT and ^{3}ILCT or $^3\pi,\pi^*$ excited states is less, or in other words, the extent of excited-state equilibrium is greater, and as a result, the contribution of ^{3}ILCT or $^3\pi,\pi^*$ excited state on the lifetime of the complexes is greater. By contrast, with an electron-withdrawing substituent (nitro-group), the contribution of ^{3}MLCT is expected to be much higher.

The reason for emission quenching upon trans−trans to trans−cis transformation is again not very clear to us. We believe that $^3\pi,\pi^*$ excited state played a definite role in the isomerization process. Conversion from trans−trans to trans−cis form imparts considerable strain and decreases π-conjugation to some extent, on and around C═C, which in turn perturbs the equilibrated ^{3}MLCT and ^{3}ILCT or $^3\pi,\pi^*$ excited states at RT.

The rate and the rate constant of the photoinduced isomerization process were evaluated from the absorption titration data. Isomerization at the initial stage of photolysis obeys first-order kinetics, as at the initial stage, the reverse isomerization rate for both photo and thermal pathway is extremely slow. Estimated rate constants vary in the range between 1.25×10^{-4} and 2.54×10^{-4} s^{-1} (Figures S43−S44, Supporting Information). The intensity of light was 0.11 W. The quantum yields of trans−trans to trans−cis conversion were calculated by adopting the process given in the experimental section of the Supporting Information. Quantum yield values are found to be low for all cases and lie in the range of 1.00×10^{-5} and 4.62×10^{-5} (Table 3). Interestingly,

Table 3. Quantum Yield and Rate Constants for the Photoisomerization of Complexes 1−5

compds	quantum yield ($\Phi \times 10^5$)	rate constant ($k_{iso} \times 10^4/s^{-1}$)
1	3.59	2.10
2	4.62	2.54
3	2.90	2.02
4	1.00	1.25
5	3.80	2.43

the rate constants as well as the quantum yields of the photoisomerization process increase systematically upon increasing the electron donating nature of X in the complexes, and a linear correlation is observed upon plotting both rate constants and quantum yields of the photoisomerization process versus Hammett σ_p parameters (Figure 11).

CONCLUSIONS

Synthesis and structural characterization of a new type of homoleptic terpyridine complexes of Ru(II) containing styrylbenzene moieties were undertaken in this work to improve the RT luminescence properties. Photophysical,

DOI: 10.1021/acsomega.8b01927
ACS Omega 2018, 3, 14526−14537

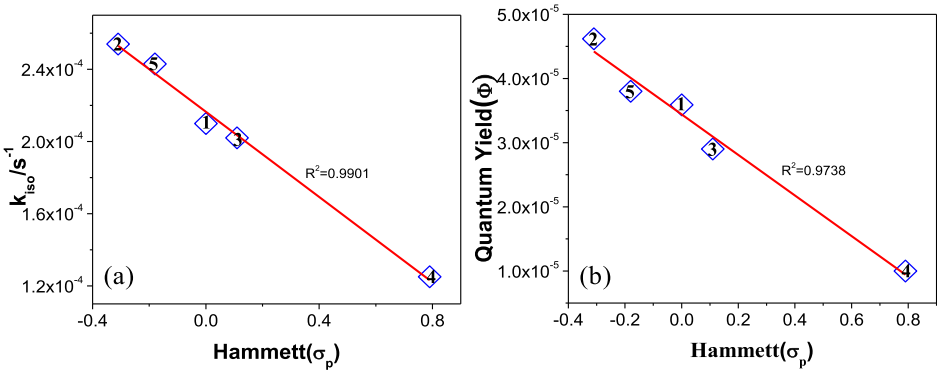

Figure 11. Plot of (a) rate constant (k_{iso}) and (b) quantum yield (Φ) of photoisomerization of the complexes vs Hammett σ_p parameters with linear least-square fits to the data.

electrochemical, and computational studies were carried out in detail. In our previous report, we demonstrated that incorporation of one styrylbenzene unit leads to the enhancement of RT lifetime up to 22.82 ns in the heteroleptic Ru(II)−terpyridine complexes. In the present study, incorporation of two styrylbenzene−terpyridine ligands provides greater electron delocalization in the excited states, resulting in substantial enhancement of the lifetime (between 10.0 and 158.5 ns, dependent on X and solvent), and the extent of enhancement is about 3 orders of magnitude higher compared with the parent $[Ru(tpy)_2]^{2+}$ complex (τ = 0.25 ns). Moreover, lifetimes in both of their trans−trans and trans−cis forms systematically varied with the electronic nature of X, yielding a good correlation with Hammett σ_p parameters. The biexponential decays indicate that the ^{3}MLCT and ^{3}IL states are in equilibrium at RT.

Another important aspect is that the presence of two styrylbenzene groups induces trans−trans to trans−cis isomerization on irradiation with UV light, resulting in considerable changes in their electronic absorption and emission spectral profiles. Reversal of the process also occurs upon interaction with visible light. Interestingly, trans−trans to trans−cis process induces emission quenching, whereas the reverse process leads to the restoration of the original emission. Thus, "on−off" and "off−on" switching of emission is feasible on treating with UV and visible light successively. Thus, the present complexes could be potential building blocks with regard to information storage and photoswitching molecular devices.

EXPERIMENTAL SECTION

Materials. The ligands tpy-pvp-X (X = H, Me, Cl, NO_2, and Ph) were synthesized and thoroughly characterized by our recent reported procedure.[89] $RuCl_3{\cdot}xH_2O$ and sodium perchlorate were purchased from Sigma. Other chemicals and solvents employed in this study were procured from local vendors.

Synthesis of Metal Complexes. Complexes were prepared by adopting a common procedure which is described below.

*$[Ru(tpy\text{-}pvp\text{-}H)_2](ClO_4)_2{\cdot}H_2O$ (**1**).* A mixture of tpy-pvp-H (0.18 g, 0.44 mmol) and $RuCl_3{\cdot}3H_2O$ (0.05 g, 0.2 mmol) in 25 mL of ethylene glycol was heated at 180 °C with stirring for 6 h under Ar atmosphere when a red solution was formed. After cooling, the solution was poured into $NaClO_4{\cdot}H_2O$ (1.5 g in 5 mL of water) and stirred for few minutes until a red-colored precipitate appeared. The compound was filtered and purified by silica gel column chromatography using MeCN as the eluent. Upon rotary evaporation of the eluent to a small volume (∼10 mL), a microcrystalline complex was formed, which was filtered and recrystallized from the MeCN−MeOH (1:5, v/v) mixture. Yield: 0.14 g (62%). Anal. Calcd for $C_{58}H_{44}N_6Cl_2O_9Ru$: C, 61.05; H, 3.89; N, 7.36. Found: C, 61.00; H, 3.91; N, 7.39. ^{1}H NMR (300 MHz, DMSO-d_6): δ/ppm 9.50 (s, 4H, 4H3′), 9.12 (d, 4H, J = 7.8 Hz, 4H6), 8.50 (d, 4H, J = 7.7 Hz, 4H7), 8.06−7.98 (m, 8H, 4H4 + 4H8), 7.81 (d, 4H, J = 7.4 Hz, 4H11), 7.58−7.47 (m, 8H, 4H3 + 4H12), 7.48 (nr, 2H, 2H13′), 7.43−7.37 (m, 4H, 2H9 + 2H10), (d, 2H, J = 7.5 Hz, 2H10), 7.28 (nr, 4H, 4H5). Electrospray ionization mass spectrometry (ESI-MS) (positive, MeCN) m/z: 462.03 (100%) $[Ru(tpy\text{-}pvp\text{-}H)_2]^{2+}$ and m/z: 1023.20 (8%) $[Ru(tpy\text{-}pvp\text{-}H)_2(ClO_4)]^+$.

*$[Ru(tpy\text{-}pvp\text{-}Me)_2](ClO_4)_2{\cdot}H_2O$ (**2**).* Yield: 0.15 g (64%). Elemental Anal. Calcd for $C_{60}H_{48}N_6Cl_2O_9Ru$: C, 61.64; H, 4.14; N, 7.19. Found: C, 61.60; H, 4.19; N, 7.22. ^{1}H NMR (300 MHz, DMSO-d_6): δ/ppm 9.50 (s, 4H, 4H3′), 9.12 (d, 4H, J = 8.0 Hz, 4H6), 8.48 (d, 4H, J = 8.41 Hz, 4H7), 8.06 (t, 4H, J = 7.8 Hz, 4H4), 7.97 (d, 4H, J = 8.1 Hz, 4H8), 7.60 (d, 4H, J = 7.8 Hz, 4H11), 7.55 (d, 4H, J = 5.8 Hz, 4H12), 7.51 (d, 2H, J = 18.0 Hz, 2H9), 7.39 (d, 2H, J = 15.0 Hz, 2H10), 7.29−7.24 (m, 8H, 4H3 + 4H5), 2.34 (s, 6H, $-CH_3$). ESI-MS (positive, MeCN) m/z: 476.04 (100%) $[Ru(tpy\text{-}pvp\text{-}Me)_2]^{2+}$ and m/z: 1051.23 (4%) $[Ru(tpy\text{-}pvp\text{-}Me)_2(ClO_4)]^+$.

*$[Ru(tpy\text{-}pvp\text{-}Cl)_2](ClO_4)_2{\cdot}H_2O$ (**3**).* Yield: 0.15 g (62%). Elemental Anal. Calcd for $C_{58}H_{42}N_6Cl_4O_9Ru$: C, 57.57; H, 3.50; N, 6.95. Found: C, 57.49; H, 3.56; N, 7.00. ^{1}H NMR (300 MHz, DMSO-d_6): δ/ppm 9.51 (s, 4H, 4H3′), 9.12 (d, 4H, J = 8.2 Hz, 4H6), 8.50 (d, 4H, J = 8.3 Hz, 4H7), 8.06 (t, 4H, J = 7.8 Hz, 4H4), 7.99 (d, 4H, J = 8.3 Hz, 4H8), 7.73 (d, 4H, J = 8.6 Hz, 4H11), 7.58−7.49 (m, 12H, 4H3 + 2H9 + 2H10, 4H12), 7.27 (t, 4H, J = 6.1 Hz, 4H5). ESI-MS (positive, MeCN) m/z: 496.96 (100%) $[Ru(tpy\text{-}pvp\text{-}Cl)_2]^{2+}$ and m/z: 1093.12 (6%) $[Ru(tpy\text{-}pvp\text{-}Cl)_2(ClO_4)]^+$.

*$[Ru(tpy\text{-}pvp\text{-}NO_2)_2](ClO_4)_2{\cdot}2H_2O$ (**4**).* Yield: 0.16 g (65%). Elemental Anal. Calcd for $C_{58}H_{44}N_8Cl_2O_{14}Ru$: C, 55.77; H, 3.55; N, 8.97. Found: C, 55.73; H, 3.62; N, 9.03. ^{1}H NMR (300 MHz, DMSO-d_6): δ/ppm 9.53 (s, 4H, 4H3′), 9.12 (d, 4H, J = 7.9 Hz, 4H6), 8.54 (d, 4H, J = 8.1 Hz, 4H7), 8.31 (d, 4H, J = 8.7 Hz, 4H12), 8.08−8.06 (m, 8H, 4H4 + 4H8), 7.96 (d, 4H, J = 8.8 Hz, 4H11), 7.72 (nr, 4H, 2H9 + 2H10), 7.56 (d, 4H, J = 5.2 Hz, 4H3), 7.28 (t, 4H, J = 5.2 Hz, 4H5). ESI-MS (positive, MeCN) m/z: 507.01 (100%) $[Ru(tpy\text{-}pvp\text{-}NO_2)_2]^{2+}$.

DOI: 10.1021/acsomega.8b01927
ACS Omega 2018, 3, 14526−14537

[Ru(tpy-pvp-Ph)$_2$](ClO$_4$)$_2$·3H$_2$O (**5**). Yield: 0.17 g (64%). Elemental Anal. Calcd for $C_{70}H_{56}N_6Cl_2O_{11}Ru$: C, 63.25; H, 4.25; N, 6.32. Found: C, 63.20; H, 4.30; N, 6.38. ^{1}H NMR (300 MHz, DMSO-d_6): δ/ppm 9.52 (s, 4H, 2H3′), 9.14 (d, 4H, J = 8.1 Hz, 4H6), 8.52 (d, 4H, J = 8.1 Hz, 4H7), 8.09−8.01 (m, 8H, 4H4 + 4H7), 7.82−7.73 (m, 12H, 4H11 + 4H13 + 4H14), 7.58−7.54 (m, 10H, 4H3 + 4H12 + 2H15), 7.49−7.38 (m, 4H, 2H9 + 2H10), 7.28 (t, 4H, J = 6.2 Hz, 4H5). ESI-MS (positive, MeCN) m/z: 538.29 (100%) [Ru(tpy-pvp-Ph)$_2$]$^{2+}$.

Caution! Perchlorate salts of the metal complexes are potentially explosive and therefore should be handled in small quantities with care.

Physical Measurements. The details of different equipment used and experimental process to measure absorption and luminescence spectral behaviors, electrochemical investigations, and computational studies using DFT and TD-DFT methods were given in the Supporting Information.

■ ASSOCIATED CONTENT

Supporting Information

The Supporting Information is available free of charge on the ACS Publications website at DOI: 10.1021/acsomega.8b01927.

DFT and TD-DFT calculated structural parameters along with figures and tables related to ESI mass, NMR, UV−vis absorption, and steady-state and time-resolved luminescence spectral change (PDF)

Crystallographic data for compound **2** (CIF)

■ AUTHOR INFORMATION

Corresponding Author

*E-mail: sbaitalik@hotmail.com, sujoy.baitalik@jadavpuruniversity.in. Phone: 91-033-2414-6666 (S.B.).

ORCID

Sujoy Baitalik: 0000-0001-9720-6889

Notes

The authors declare no competing financial interest.

■ ACKNOWLEDGMENTS

S.B. acknowledges the financial support received from SERB-DST (grant no. EMR/2015/001163) and CSIR (grant no. 01(7619)/18/EMR-II), New Delhi, India. P.P. and S.M. acknowledge CSIR for their research fellowship. Thanks are also due to DST for proving single-crystal X-ray diffractometer in FIST and TCSPC facility under PURSE program at the Department of Chemistry of Jadavpur University.

■ REFERENCES

(1) *Photochromic Materials: Preparation, Properties and Applications*; Tian, H., Zhang, J., Eds.; Wiley-VCH: Weinheim, Germany, 2016.

(2) Ko, C.-C.; Yam, V. W.-W. Coordination compounds with photochromic ligands: ready tunability and visible light-sensitized photochromism. *Acc. Chem. Res.* **2018**, *51*, 149−159.

(3) *Organic Photochromic and Thermochromic Compounds, Vol 1: Main Photochromic Families*; Crano, J. C., Guglielmetti, R., Eds.; Plenum Press: New York, 1999.

(4) *Organic Photochromic and Thermochromic Compounds, Vol 2: Physicochemical Studies, Biological Applications and Thermochromism*; Crano, J. C., Guglielmetti, R., Eds.; Plenum Press: New York, 1999.

(5) Feringa, B. L.; Van Delden, R. A.; Ter Wiel, M. K. J. In *Chiroptical Molecular Switches in Molecular Switches*; Feringa, B. L., Ed.; Wiley-VCH: Weinheim, 2001; pp 123−163.

(6) Kawata, S.; Kawata, Y. Three-dimensional optical data storage using photochromic materials. *Chem. Rev.* **2000**, *100*, 1777−1788.

(7) Rau, H. In *Photochromism: Molecules and Systems*; Dürr, H., Laurent, H. B., Eds.; Elsevier: Amsterdam, 1990; pp 165−192.

(8) Ikeda, T.; Tsutsumi, O. Optical switching and image storage by means of azobenzene liquid-crystal films. *Science* **1995**, *268*, 1873−1875.

(9) Waldeck, D. H. Photoisomerization dynamics of stilbenes. *Chem. Rev.* **1991**, *91*, 415−436.

(10) Momotake, A.; Arai, T. Photochemistry and photophysics of stilbene dendrimers and related compounds. *J. Photochem. Photobiol., C* **2004**, *5*, 1−25.

(11) Irie, M. Diarylethenes for memories and switches. *Chem. Rev.* **2000**, *100*, 1685−1716.

(12) Tian, H.; Yang, S. Recent progresses on diarylethene based photochromic switches. *Chem. Soc. Rev.* **2004**, *33*, 85−97.

(13) Matsuda, K.; Irie, M. Diarylethene as a photoswitching unit. *J. Photochem. Photobiol., C* **2004**, *5*, 169−182.

(14) Kume, S.; Nishihara, H. Photochrome-coupled metal complexes: molecular processing of photon stimuli. *Dalton Trans.* **2008**, 3260−3271.

(15) Kurihara, M.; Nishihara, H. Azo- and quinone-conjugated redox complexes-photo- and proton-coupled intramolecular reactions based on d-π interaction. *Coord. Chem. Rev.* **2002**, *226*, 125−135.

(16) Nishihara, H. Multi-mode molecular switching properties and functions of azo-conjugated metal complexes. *Bull. Chem. Soc. Jpn.* **2004**, *77*, 407−428.

(17) Nishihara, H. *Inorganic Photochromism*; Kodansha, Y. F., Ed.; Springer, 2007; pp 239−257.

(18) Kume, S.; Nishihara, H. Metal-based photoswitches derived from photoisomerization. *Struct. Bonding* **2007**, *123*, 79−112.

(19) Ko, C.-C.; Wing-Wah Yam, V. Transition metal complexes with photochromic ligands−photosensitization and photoswitchable properties. *J. Mater. Chem.* **2010**, *20*, 2063−2070.

(20) Ko, C.-C.; Wu, L.-X.; Wong, K. M.-C.; Zhu, N.; Yam, V. W.-W. Synthesis, Characterization and Photochromic Studies of Spirooxazine-Containing 2,2′-Bipyridine Ligands and Their Rhenium(i) Tricarbonyl Complexes. *Chem.—Eur. J.* **2004**, *10*, 766−776.

(21) Li, Y.; Tam, A. Y.-Y.; Wong, K. M.-C.; Li, W.; Wu, L.; Yam, V. W.-W. Synthesis, characterization, and the photochromic, luminescence, metallogelation and liquid-crystalline properties of multifunctional platinum(II) bipyridine complexes. *Chem.—Eur. J.* **2011**, *17*, 8048−8059.

(22) Ko, C.-C.; Kwok, W.-M.; Yam, V. W.-W.; Phillips, D. L. Triplet MLCT Photosensitization of the ring-closing reaction of diarylethenes by design and synthesis of a photochromic Rhenium(I) complex of a diarylethene-containing 1,10-phenanthroline ligand. *Chem.—Eur. J.* **2006**, *12*, 5840−5848.

(23) Lee, P. H.-M.; Ko, C.-C.; Zhu, N.; Yam, V. W.-W. Metal Coordination-assisted near-Infrared photochromic behavior: a large perturbation on absorption wavelength properties of N,N-donor ligands containing diarylethene derivatives by coordination to the rhenium(I) metal center. *J. Am. Chem. Soc.* **2007**, *129*, 6058−6059.

(24) Chan, J. C.-H.; Lam, W. H.; Wong, H.-L.; Zhu, N.; Wong, W.-T.; Yam, V. W.-W. Diarylethene-containing cyclometalated platinum-(II) complexes: tunable photochromism via metal coordination and rational ligand design. *J. Am. Chem. Soc.* **2011**, *133*, 12690−12705.

(25) Alstrum-Acevedo, J. H.; Brennaman, M. K.; Meyer, T. J. Chemical Approaches to Artificial Photosynthesis. 2. *Inorg. Chem.* **2005**, *44*, 6802−6827.

(26) Evans, R. C.; Douglas, P.; Winscom, C. J. Coordination complexes exhibiting room-temperature phosphorescence: evaluation of their suitability as triplet emitters in organic light emitting diodes. *Coord. Chem. Rev.* **2006**, *250*, 2093−2126.

(27) Campagna, S.; Puntoriero, F.; Nastasi, F.; Bergamini, G.; Balzani, V. In *Photochemistry and Photophysics of Coordination Compounds I*; Topics in Current Chemistry; Balzani, V., Campagna, S., Eds.; Springer, 2007; Vol. *280*, pp 117−214.

DOI: 10.1021/acsomega.8b01927
ACS Omega 2018, 3, 14526−14537

(28) Yersin, H.; Rausch, A. F.; Czerwieniec, R.; Hofbeck, T.; Fischer, T. The triplet state of organo-transition metal compounds. triplet harvesting and singlet harvesting for efficient OLEDs. *Coord. Chem. Rev.* **2011**, *255*, 2622−2652.
(29) Hardy, J. G. Metallosupramolecular grid complexes: towards nanostructured materials with high-tech applications. *Chem. Soc. Rev.* **2013**, *42*, 7881−7899.
(30) Baggaley, E.; Botchway, S. W.; Haycock, J. W.; Morris, H.; Sazanovich, I. V.; Williams, J. A. G.; Weinstein, J. A. Long-lived metal complexes open up microsecond lifetime imaging microscopy under multiphoton excitation: from FLIM to PLIM and beyond. *Chem. Sci.* **2014**, *5*, 879−886.
(31) Sun, S.-S.; Robson, E.; Dunwoody, N.; Silva, A. S.; Lees, A. J.; Brinn, I. M. Photoswitchable trinuclear transition-metal complexes. Intramolecular triplet−triplet energy transfer from *fac*-(diimine)ReI-$(CO)_3$ chromophores to a stilbene-like bridging ligand. *Chem. Commun.* **2000**, 201−202.
(32) Lin, J.-L.; Chen, C.-W.; Sun, S.-S.; Lees, A. J. Photoswitching tetranuclear rhenium(I) tricarbonyl diimine complexes with a stilbene-like bridging ligand. *Chem. Commun.* **2011**, *47*, 6030−6032.
(33) Sun, S.-S.; Anspach, J. A.; Lees, A. J. Self-Assembly of Transition-Metal-Based Macrocycles Linked by Photoisomerizable Ligands: Examples of Photoinduced Conversion of Tetranuclear−Dinuclear Squares. *Inorg. Chem.* **2002**, *41*, 1862−1869.
(34) Price, R. S.; Dubinina, G.; Wicks, G.; Drobizhev, M.; Rebane, A.; Schanze, K. S. Polymer monoliths containing two-photon absorbing phenylenevinylene platinum(II) acetylide chromophores for optical power limiting. *ACS Appl. Mater. Interfaces* **2015**, *7*, 10795−10805.
(35) Haskins-Glusac, K.; Ghiviriga, I.; Abboud, K. A.; Schanze, K. S. Photophysics and photochemistry of stilbene-containing platinum acetylides. *J. Phys. Chem. B* **2004**, *108*, 4969−4978.
(36) Yao, L.-Y.; Yam, V. W.-W. Photoinduced isomerization-driven structural transformation between decanuclear and octadecanuclear gold(I) sulfido clusters. *J. Am. Chem. Soc.* **2015**, *137*, 3506−3509.
(37) Yam, V. W.-W.; Yang, Y.; Zhang, J.; Chu, B. W.-K.; Zhu, N. Synthesis, characterization, and photoisomerization studies of azo- and stilbene-containing surfactant rhenium(I) complexes. *Organometallics* **2001**, *20*, 4911−4918.
(38) Juris, A.; Balzani, V.; Barigelletti, F.; Campagna, S.; Belser, P.; von Zelewsky, A. Ru(II) polypyridine complexes: photophysics, photochemistry, eletrochemistry, and chemiluminescence. *Coord. Chem. Rev.* **1988**, *84*, 85−277.
(39) Sauvage, J. P.; Collin, J. P.; Chambron, J. C.; Guillerez, S.; Coudret, C.; Balzani, V.; Barigelletti, F.; De Cola, L.; Flamigni, L. Ruthenium(II) and osmium(II) bis(terpyridine) complexes in covalently-linked multicomponent systems: synthesis, electrochemical behavior, absorption spectra, and photochemical and photophysical properties. *Chem. Rev.* **1994**, *94*, 993−1019.
(40) Browne, W. R.; O'Boyle, N. M.; McGarvey, J. J.; Vos, J. G. Elucidating excited state electronic structure and intercomponent interactions in multicomponent and supramolecular systems. *Chem. Soc. Rev.* **2005**, *34*, 641−663.
(41) Williams, J. A. G. The coordination chemistry of dipyridylbenzene: N-deficient terpyridine or panacea for brightly luminescent metal complexes? *Chem. Soc. Rev.* **2009**, *38*, 1783−1801.
(42) Pal, A. K.; Hanan, G. S. Design, synthesis and excited-state properties of mononuclear Ru(II) complexes of tridentate heterocyclic ligands. *Chem. Soc. Rev.* **2014**, *43*, 6184−6197.
(43) Medlycott, E. A.; Hanan, G. S. Synthesis and properties of mono- and oligo-nuclear Ru(II) complexes of tridentate ligands: the quest for long-lived excited states at room temperature. *Coord. Chem. Rev.* **2006**, *250*, 1763−1782.
(44) Hofmeier, H.; Schubert, U. S. Recent developments in the supramolecular chemistry of terpyridine-metal complexes. *Chem. Soc. Rev.* **2004**, *33*, 373−399.
(45) Constable, E. C. 2,2′:6′,2″-Terpyridines: From chemical obscurity to common supramolecular motifs. *Chem. Soc. Rev.* **2007**, *36*, 246−253.
(46) Harriman, A.; Ziessel, R. Making photoactive molecular-scale wires. *Chem. Commun.* **1996**, 1707−1716.
(47) Breivogel, A.; Kreitner, C.; Heinze, K. Redox and Photochemistry of Bis(terpyridine)ruthenium(II) Amino Acids and Their Amide Conjugates - from Understanding to Applications. *Eur. J. Inorg. Chem.* **2014**, 5468−5490.
(48) Winkler, J. R.; Netzel, T. L.; Creutz, C.; Sutin, N. Direct observation of metal-to-ligand charge-transfer (MLCT) excited states of pentaammineruthenium(II) complexes. *J. Am. Chem. Soc.* **1987**, *109*, 2381−2392.
(49) Wang, J.; Fang, Y.-Q.; Hanan, G. S.; Loiseau, F.; Campagna, S. Synthesis and Properties of the Elusive Ruthenium(II) Complexes of 4'-Cyano-2,2′:6′,2″-terpyridine. *Inorg. Chem.* **2005**, *44*, 5−7.
(50) Kübel, J.; Schroot, R.; Wächtler, M.; Schubert, U. S.; Dietzek, B.; Jäger, M. Photoredox-active dyads based on a Ru(II) photosensitizer equipped with electron donor or acceptor polymer chains: a spectroscopic study of light-induced processes toward efficient charge separation. *J. Phys. Chem. C* **2015**, *119*, 4742−4751.
(51) Maestri, M.; Armaroli, N.; Balzani, V.; Constable, E. C.; Thompson, A. M. W. C. Complexes of the ruthenium(II)-2,2':6',2''-terpyridine family. effect of electron-accepting and -donating substituents on the photophysical and electrochemical properties. *Inorg. Chem.* **1995**, *34*, 2759−2767.
(52) Fang, Y.-Q.; Taylor, N. J.; Hanan, G. S.; Loiseau, F.; Passalacqua, R.; Campagna, S.; Nierengarten, H.; Van Dorsselaer, A. V. A strategy for improving the room-temperature luminescence properties of Ru(II) complexes with tridentate ligands. *J. Am. Chem. Soc.* **2002**, *124*, 7912−7913.
(53) Encinas, S.; Flamigni, L.; Barigelletti, F.; Constable, E. C.; Housecroft, C. E.; Schofield, E. R.; Figgemeier, E.; Fenske, D.; Neuburger, M.; Vos, J. G.; Zehnder, M. Electronic Energy Transfer and Collection in Luminescent Molecular Rods Containing Ruthenium(II) and Osmium(II) 2,2′:6′,2″-Terpyridine Complexes Linked by Thiophene-2,5-diyl Spacers. *Chem.—Eur. J.* **2002**, *8*, 137−150.
(54) Duati, M.; Tasca, S.; Lynch, F. C.; Bohlen, H.; Vos, J. G.; Stagni, S.; Ward, M. D. Enhancement of Luminescence Lifetimes of Mononuclear Ruthenium(II)−Terpyridine Complexes by Manipulation of the σ-Donor Strength of Ligands. *Inorg. Chem.* **2003**, *42*, 8377−8384.
(55) Dietrich, J.; Thorenz, U.; Förster, C.; Heinze, K. Effects of Sequence, Connectivity, and Counter Ions in New Amide-Linked Ru(tpy)2-Re(bpy) Chromophores on Redox Chemistry and Photophysics. *Inorg. Chem.* **2013**, *52*, 1248−1264.
(56) Wadman, S. H.; Lutz, M.; Tooke, D. M.; Spek, A. L.; Hartl, F.; Havenith, R. W. A.; van Klink, G. P. M.; van Koten, G. Consequences ofN,C,N′- andC,N,N′-Coordination Modes on Electronic and Photophysical Properties of Cyclometalated Aryl Ruthenium(II) Complexes. *Inorg. Chem.* **2009**, *48*, 1887−1900.
(57) Kreitner, C.; Erdmann, E.; Seidel, W. W.; Heinze, K. Understanding the excited state behavior of cyclometalated bis-(tridentate)ruthenium(II) complexes: a combined experimental and theoretical study. *Inorg. Chem.* **2015**, *54*, 11088−11104.
(58) Shao, J.-Y.; Zhong, Y.-W. Tuning the electronic coupling in cyclometalated diruthenium complexes through substituent effects: a correlation between the experimental and calculated results. *Chem.—Eur. J.* **2014**, *20*, 8702−8713.
(59) Sinn, S.; Schulze, B.; Friebe, C.; Brown, D. G.; Jäger, M.; Kübel, J.; Dietzek, B.; Berlinguette, C. P.; Schubert, U. S. A heteroleptic bis(tridentate) ruthenium(II) platform featuring an anionic 1,2,3-triazolate-based ligand for application in the dye-sensitized solar cell. *Inorg. Chem.* **2014**, *53*, 1637−1645.
(60) Brown, D. G.; Sanguantrakun, N.; Schulze, B.; Schubert, U. S.; Berlinguette, C. P. Bis(tridentate) Ruthenium-Terpyridine Complexes Featuring Microsecond Excited-State Lifetimes. *J. Am. Chem. Soc.* **2012**, *134*, 12354−12357.
(61) Fang, Y.-Q.; Taylor, N. J.; Laverdière, F.; Hanan, G. S.; Loiseau, F.; Nastasi, F.; Campagna, S.; Nierengarten, H.; Leize-Wagner, E.; Van Dorsselaer, A. Ruthenium(II) Complexes with Improved

DOI: 10.1021/acsomega.8b01927
ACS Omega 2018, 3, 14526−14537

Photophysical Properties Based on Planar 4′-(2-Pyrimidinyl)-2,2′:6′,2″-terpyridine Ligands. *Inorg. Chem.* **2007**, *46*, 2854−2863.
(62) Passalacqua, R.; Loiseau, F.; Campagna, S.; Fang, Y.-Q.; Hanan, G. S. In search of ruthenium(II) complexes based on tridentate polypyridine ligands that feature long-lived room-temperature luminescence: the multichromophore approach. *Angew. Chem., Int. Ed.* **2003**, *42*, 1608−1611.
(63) Schlotthauer, T.; Suchland, B.; Görls, H.; Parada, G. A.; Hammarström, L.; Schubert, U. S.; Jäger, M. Aryl-decorated Ru^{II} polypyridyl-type photosensitizer approaching NIR emission with microsecond excited state lifetimes. *Inorg. Chem.* **2016**, *55*, 5405−5416.
(64) Abrahamsson, M.; Jäger, M.; Kumar, R. J.; Österman, T.; Persson, P.; Becker, H.-C.; Johansson, O.; Hammarström, L. Bistridentate Ruthenium(II)polypyridyl-Type Complexes with Micro-second3MLCT State Lifetimes: Sensitizers for Rod-Like Molecular Arrays. *J. Am. Chem. Soc.* **2008**, *130*, 15533−15542.
(65) Wang, X.-Y.; Del Guerzo, A.; Tunuguntla, H.; Schmehl, R. H. Photophysical behavior of Ru(II) and Os(II) terpyridyl phenylene vinylene complexes: perturbation of MLCT state by intra-ligand charge-transfer state. *Res. Chem. Intermed.* **2007**, *33*, 63−77.
(66) Siebert, R.; Winter, A.; Schubert, U. S.; Dietzek, B.; Popp, J. The molecular mechanism of dual emission in terpyridine transition metal complexes—ultrafast investigations of photoinduced dynamics. *Phys. Chem. Chem. Phys.* **2011**, *13*, 1606−1617.
(67) Preiß, J.; Jäger, M.; Rau, S.; Dietzek, B.; Popp, J.; Martínez, T.; Presselt, M. How does peripheral functionalization of ruthenium(II)-terpyridine complexes affect spatial charge redistribution after photoexcitation at the franck-condon point? *ChemPhysChem* **2015**, *16*, 1395−1404.
(68) Hissler, M.; El-ghayoury, A.; Harriman, A.; Ziessel, R. Fine-tuning the electronic properties of binuclear bis(terpyridyl)-ruthenium(II) complexes. *Angew. Chem., Int. Ed.* **1998**, *37*, 1717−1720.
(69) Breivogel, A.; Förster, C.; Heinze, K. A heteroleptic bis(tridentate)ruthenium(II) polypyridine complex with improved photophysical properties and integrated functionalizability. *Inorg. Chem.* **2010**, *49*, 7052−7056.
(70) Leslie, W.; Batsanov, A. S.; Howard, J. A. K.; Williams, J. A. G. Cross-couplings in the elaboration of luminescent bis-terpyridyl iridium complexes: the effect of extended or inhibited conjugation on emission. *Dalton Trans.* **2004**, 623−631.
(71) Arm, K. J.; Williams, J. A. G. A cross-coupling strategy for the synthesis of dimetallic assemblies containing mixed bipyridine−terpyridine bridging ligands: luminescence and energy transfer properties. *Dalton Trans.* **2006**, 2172−2174.
(72) Mondal, D.; Bar, M.; Mukherjee, S.; Baitalik, S. Design of Ru(II) complexes based on anthraimidazoledione-functionalized terpyridine ligand for improvement of room-temperature luminescence characteristics and recognition of selective anions: experimental and DFT/TD-DFT study. *Inorg. Chem.* **2016**, *55*, 9707−9724.
(73) Karmakar, S.; Maity, D.; Mardanya, S.; Baitalik, S. Multichromophoric bimetallic Ru(II) terpyridine complexes based on pyrenyl-bis-phenylimidazole spacer: synthesis, photophysics, spectroelectrochemistry, and TD-DFT calculations. *Inorg. Chem.* **2014**, *53*, 12036−12049.
(74) Maity, D.; Bhaumik, C.; Mardanya, S.; Karmakar, S.; Baitalik, S. Light Harvesting and Directional Energy Transfer in Long-Lived Homo- and Heterotrimetallic Complexes of FeII, RuII, and OsII. *Chem.—Eur. J.* **2014**, *20*, 13242−13252.
(75) Maity, D.; Bhaumik, C.; Mondal, D.; Baitalik, S. Ru(II) and Os(II) complexes based on terpyridyl-imidazole ligand rigidly linked to pyrene: synthesis, structure, photophysics, electrochemistry, and anion-sensing studies. *Inorg. Chem.* **2013**, *52*, 13941−13955.
(76) Maity, D.; Das, S.; Mardanya, S.; Baitalik, S. Synthesis, Structural Characterization, and Photophysical, Spectroelectrochemical, and Anion-Sensing Studies of Heteroleptic Ruthenium(II) Complexes Derived from 4′-Polyaromatic-Substituted Terpyridine Derivatives and 2,6-Bis(benzimidazol-2-yl)pyridine. *Inorg. Chem.* **2013**, *52*, 6820−6838.
(77) Bhaumik, C.; Saha, D.; Das, S.; Baitalik, S. Synthesis, structural characterization, photophysical, electrochemical, and anion-sensing studies of luminescent homo- and heteroleptic ruthenium(II) and osmium(II) complexes based on terpyridyl-imidazole ligand. *Inorg. Chem.* **2011**, *50*, 12586−12600.
(78) Karmakar, S.; Mardanya, S.; Das, S.; Baitalik, S. Efficient Deep-Blue Emittier and Molecular-Scale Memory Device Based on Dipyridyl-Phenylimidazole-Terpyridine Assembly. *J. Phys. Chem. C* **2015**, *119*, 6793−6805.
(79) Mondal, D.; Biswas, S.; Paul, A.; Baitalik, S. Luminescent dinuclear ruthenium terpyridine complexes with a bis-phenyl-benzimidazole spacer. *Inorg. Chem.* **2017**, *56*, 7624−7641.
(80) Bhaumik, C.; Das, S.; Saha, D.; Dutta, S.; Baitalik, S. Synthesis, Characterization, Photophysical, and Anion-Binding Studies of Luminescent Heteroleptic Bis-Tridentate Ruthenium(II) Complexes Based on 2,6-Bis(Benzimidazole-2-yl)Pyridine and 4′-Substituted 2,2′:6′,2″ Terpyridine Derivatives. *Inorg. Chem.* **2010**, *49*, 5049−5062.
(81) Bhaumik, C.; Das, S.; Maity, D.; Baitalik, S. Luminescent bis-tridentate ruthenium(II) and osmium(II) complexes based on terpyridyl-imidazole ligand: synthesis, structural characterization, photophysical, electrochemical, and solvent dependence studies. *Dalton Trans.* **2012**, *41*, 2427−2438.
(82) Takahashi, K.; Hasegawa, Y.; Sakamoto, R.; Nishikawa, M.; Kume, S.; Nishibori, E.; Nishihara, H. Solid-state ligand-driven light-induced spin change at ambient temperatures in bis(dipyrazolylstyrylpyridine)iron(II) complexes. *Inorg. Chem.* **2012**, *51*, 5188−5198.
(83) Hasegawa, Y.; Takahashi, K.; Kume, S.; Nishihara, H. Complete solid state photoisomerization of bis(dipyrazolylstyrylpyridine)iron-(II) to change magnetic properties. *Chem. Commun.* **2011**, *47*, 6846−6848.
(84) Sakamoto, R.; Murata, M.; Kume, S.; Sampei, H.; Sugimoto, M.; Nishihara, H. Photo-controllable tristability of a dithiolato-bipyridine-Pt(II) complex molecule containing two azobenzene moieties. *Chem. Commun.* **2005**, 1215−1217.
(85) Kume, S.; Kurihara, M.; Nishihara, H. Reversible *trans-cis* photoisomerization of azobenzene-attached bipyridine ligands coordinated to cobalt using a single UV light source and the Co(III)/Co(II) redox change. *Chem. Commun.* **2001**, 1656−1657.
(86) Yutaka, T.; Mori, I.; Kurihara, M.; Mizutani, J.; Tamai, N.; Kawai, T.; Irie, M.; Nishihara, H. Photoluminescence Switching of Azobenzene-Conjugated Pt(II) Terpyridine Complexes by Trans−Cis Photoisomerization. *Inorg. Chem.* **2002**, *41*, 7143−7150.
(87) Yutaka, T.; Kurihara, M.; Kubo, K.; Nishihara, H. Novel photoisomerization behavior of Rh binuclear complexes involving an azobenzene-bridged bis(terpyridine) ligand. Strong effects of counter-ion and solvent and the induction of redox potential shift. *Inorg. Chem.* **2000**, *39*, 3438−3439.
(88) Yutaka, T.; Mori, I.; Kurihara, M.; Mizutani, J.; Kubo, K.; Furusho, S.; Matsumura, K.; Tamai, N.; Nishihara, H. Synthesis, characterization, and photochemical properties of azobenzene-conjugated Ru(II) and Rh(III) bis(terpyridine) complexes. *Inorg. Chem.* **2001**, *40*, 4986−4995.
(89) Pal, P.; Mukherjee, S.; Maity, D.; Baitalik, S. Synthesis, Structural Characterization, and Luminescence Switching of Diarylethene-Conjugated Ru(II)-Terpyridine Complexes by *trans-cis* Photoisomerization: Experimental and DFT/TD-DFT Investigation. *Inorg. Chem.* **2018**, *57*, 5743−5753.
(90) Hansch, C.; Leo, A.; Taft, R. W. A survey of Hammett substituent constants and resonance and field parameters. *Chem. Rev.* **1991**, *91*, 165−195.

DOI: 10.1021/acsomega.8b01927
ACS Omega 2018, 3, 14526−14537